J. Fluid Mech. (1986), *vol.* 162, *pp.* 439–462
Printed in Great Britain

On the magnitude of the subgrid-scale eddy coefficient in large-eddy simulations of turbulent channel flow

By P. J. MASON AND N. S. CALLEN
Meteorological Office, London Road, Bracknell, Berkshire RG12 2SZ

(Received 17 October 1984 and in revised form 6 September 1985)

A series of large-eddy simulations of plane Poiseuille flow are discussed. The subgrid-scale motions are represented by an eddy viscosity related to the flow deformation – the 'Smagorinsky' model. The resolution of the computational mesh is varied independently of the value of the coefficient C_s which determines the magnitude of this subgrid eddy viscosity. To ensure that results are from a statistically steady state unrealistic initial conditions are used and sufficient time is allowed for the flow to become independent of the initial conditions. In keeping with previous work it is found that for large C_s the resolved-scale motions are damped out; however, this critical value of C_s is found to depend on the mesh resolution. Only with a fine mesh does the value of C_s previously found to be appropriate for homogeneous turbulence (≈ 0.2) give simulations with sustained resolved-scale motions. The ratio l_0/δ of the channel width 2δ to the scale of the 'Smagorinsky' mixing length, $l_0 = C_s \Delta$ where Δ is a typical mesh spacing), is found to be the key parameter determining the 'turbulent' eddy-viscosity 'Reynolds number' of the resolved-scale motions. A fixed value of l_0 is regarded as determining the separation of scales into resolved and subgrid. The value of C_s is regarded as a measure of numerical resolution and values of C_s less than about 0.2 correspond to inadequate resolution.

1. Introduction

In many turbulent flows it is clear that the flow properties are dominated by the influence of large-scale turbulent eddies. Such eddies produce turbulent transports which depend on the gross character of the flow and have a very indirect relationship to the local mean-flow structure. The failure of time-average turbulence closure techniques, whether simple eddy-viscosity models or complex high-order closure techniques, is often related to this difficulty. The advent of computers powerful enough to compute three-dimensional time-dependent flows has allowed the development of large-eddy-turbulence simulation. This technique involves calculating the large-scale (resolved-scale) turbulent motions explicitly and attempting to parametrize the effects of the small-scale (subgrid-scale) motions. Provided that the main scales of motion involved in turbulence energy production are resolved by the numerical model, there are two reasons contributing to the success of such an approach. First, as the model resolves most of the energy-containing eddies, the results might be anticipated to be insensitive to the details of how the small-scale motions are dealt with. Secondly, it is observed that, while large-scale eddies differ considerably between flows, the small-scale motions hardly change in character. The small-scale

motions are generally more isotropic than the large-scale motions and may thus be parametrized more rationally.

Previous studies with large-eddy models have considered a range of different flows. Notable examples are homogeneous isotropic turbulence (McMillan & Ferziger 1979; Antonopoulos-Domis 1981), buoyant convection (Deardorff 1974) and turbulent channel flow (Moin & Kim 1982, referred to hereinafter as M & K). The studies of homogeneous turbulence have given encouraging and relatively straightforward results. The subgrid-scale motions have been parametrized using the eddy-viscosity formulation originally proposed by Smagorinsky (1963). This formulation (see (2.3)–(2.7) below) requires a value for the constant C_s relating the 'mixing-length' scale of the parametrization to the mesh scale of the numerical simulation. Lilly (1967) applied the usual local-equilibrium-turbulence arguments to deduce, from the spectrum of homogeneous turbulence, a value for C_s of about 0.23. Recently Antonopoulos-Domis (1981) has confirmed that the averaging operators implicitly involved in second-order-accurate finite-difference approximations are consistent with this value. With this value of C_s, and meshes varying from 16^3 to 64^3 grid points, the large-eddy simulations appears to give an accurate description of the decay of homogeneous turbulence. With the limited number of mesh points available for practical calculations the effective 'turbulent' Reynolds number, based on the magnitude of the Smagorinsky eddy viscosity and the amplitude of the larger-scale flow components, is always low and typically a few hundred. It is consequently impossible to resolve much of the inertial subrange and the calculated rates of decay of homogeneous turbulence should depend on this 'turbulent' Reynolds number. The dependence of the decay rate upon the values of C_s is precisely this effect. When comparing calculated rates of decay with measured values, the data are usually 'filtered' to remove scales not explicitly resolved by the computational mesh. As we shall discuss, the basis for choosing the lengthscale and form of the filter applied to the data requires a clear understanding of what scales the simulation actually represents.

The large-eddy simulations of buoyant convection (e.g. Deardorff 1974) are very impressive and provide good agreement with observations in a case where time-averaged techniques fail. The same value of C_s as used in homogeneous turbulence studies is found appropriate. The corresponding value for use in the temperature equation is less certain but not the subject of concern here.

In contrast to studies of homogeneous turbulence and buoyant convection, the studies of large-eddy simulations of turbulent channel flow have proved more difficult to conduct successfully. The instability mechanism driving the turbulent eddies (Orszag & Kells 1980) is nonlinear in character and the ability of numerical simulations to sustain initial turbulence depends on the structure and intensity of initial perturbations. Also, in contrast to the simulation of buoyant convection, the results seem relatively sensitive to the value of C_s. In past studies the resolved-scale motions have been found to damp out with values of C_s appropriate to homogeneous turbulence. In the earliest study by Deardorff (1970*b*) using 6720 grid points $C_s = 0.17$ was found to damp resolved motions and $C_s = 0.1$ was judged to be optimum. Smaller values of C_s gave excessive turbulence energy. In spite of the coarse numerical mesh the results were encouraging and gave good agreement with the experimental data of Laufer (1951). The difficulty in reconciling the value of C_s used to obtain these results with that used in simulations of homogeneous turbulence was noted by Deardorff (1970*a*) who suggested that C_s might be reduced by the flow rotation occurring near the wall. Bardina, Ferziger & Reynolds (1983) confirm the suggestion

that rotation influences the decay of turbulence but retain the usual 'homogeneous' value of C_s in their large-eddy simulation of such decay. Although further work on this point is needed, the present results provide an alternative explanation of the apparent need for small values of C_s.

Following Deardorff (1970*b*), Schumann (1975) calculated turbulent channel flow with 65536 grid points. In an effort to circumvent the tendency for resolved-scale motions to damp out he proposed, with limited theoretical support, that it might be appropriate to divide the subgrid-scale parametrized stresses into a locally 'isotropic' part with the local spatially meaned shear removed from its derivation, and an 'inhomogeneous' part derived from the mean shear. The 'inhomogeneous' part dominated close to the wall whilst in the interior the homogeneous part dominated and the value of C_s was 0.1. With this subgrid model, resolved eddies are essential to maintain a shear stress in the flow interior. Should the resolved eddies decay the shear stress will diminish, and the mean flow will accelerate under the action of the basic pressure gradient until the resolved eddies are enhanced. With the usual 'Smagorinsky' formulation the increase in mean flow is limited by a value of mean flow at which the subgrid stresses can balance the basic pressure gradient. This arbitrary neglect of the influence of mean shear on subgrid-scale turbulence in the flow interior thus encourages the simulation to maintain resolved-scale eddies. These results showed the same promise as Deardorff's (1970*b*) study and the technique was more robust. Schumann (1975) also considered the use of transport equations for subgrid-scale energy but found no improvement over the eddy-viscosity model.

A further limitation of these simulations of channel flow concerns the boundary conditions. In the real channel these correspond to turbulent flow over a no-slip surface which may be smooth or rough. We shall argue that if the distance of the nearest grid point to the wall is sufficiently small then it is correct to assume that the usual, but local, 'law-of-the-wall' relations will apply to the instantaneous resolved-scale flow. For this to be correct and to give results identical with those obtained with resolution of a mixing-length parametrization and a non-slip condition, two requirements must be satisfied. First, time dependence, pressure gradients and nonlinear accelerations must be negligible and, secondly, the grid point must represent an area of sufficient size parallel to the wall for a statistically steady stress to occur. Deardorff (1970*b*) and Schumann (1975) acknowledge that they fail to meet such criteria and use boundary conditions which are only correct for the mean flow. Schumann's (1975) boundary condition also provides an unphysical constraint on the flow. At all times the space-average wall stress is compelled to be equal to the time-average value. The mass flux through the channel is thus held at its initial prescribed value.

Moin, Reynolds & Ferziger (1978) conducted a simulation with greatly improved resolution in the direction normal to the channel walls. They provided much more than enough resolution to allow the consistent application of a locally determined 'constant-stress' solution, i.e. 'law of the wall', and resolve a viscous sublayer which allows a simple no-slip condition. As the wall is approached the lengthscale in the subgrid parametrization decreased in accord with a Prandtl mixing-length formulation. The match to a Prandtl mixing length is intended to represent the small-scale eddies which, at high Reynolds numbers, carry the shear stress near the wall. Although such eddies are anisotropic they are essentially three-dimensional with scales of order that, implied by the Prandtl mixing length and because of the limitations in resolution parallel to the wall, cannot be explicitly described in a practical simulation. The resolved motions close to the wall retain the scale of the

mesh parallel to the wall and are essentially two-dimensional and parallel to the wall. In the interior of the flow, Moin *et al.* used a Smagorinsky subgrid model with a value of $C_s = 0.09$. They obtained promising results but concluded that more resolution (greater than 16 points) was required in the spanwise direction. The most successful simulation is due to M & K and followed, with extensive modifications, the study of Moin *et al.* (1978). They used up to 516096 grid points and a subgrid model similar to that proposed by Schumann (1975). As with Moin *et al.* (1978) very fine resolution was used near the wall and the match to a viscous sublayer was achieved by using Van Driest (1956) exponential damping functions. As it involves the value of time-averaged stress this match is not locally exact.

In addition to the problem noted above the various authors express differences of opinion regarding both the need for filter functions to separate resolved and subgrid scales and also the details of the terms requiring a subgrid model (e.g. Kwak, Reynolds & Ferziger 1975). It is argued that, as demonstrated by Leonard (1974), the application of analytic filter functions to continuous variables demands terms other than those correponding to the usual Reynolds stresses. These extra terms, the 'Leonard' stresses, are beneficial with accurate high-order finite-difference schemes. However, their inclusion is not consistent in second-order-accurate schemes and it has been suggested that in such cases the Leonard (Schumann 1975; Antonopoulos-Domis 1981) terms are implicitly included or zero. We adopt a second-order-accurate numerical scheme and thus do not consider explicit Leonard-stress terms. However, we shall support the view that the filter function should be considered separate from the resolution of the finite-difference mesh.

The statistical theories of isotropic turbulence also provide models for the subgrid-scale stresses (Kraichnan 1976; Leslie & Quarini 1979). These models are more naturally applied in a spectral representation of the resolved turbulence. When developed to apply in more general conditions (e.g. Cambon, Jeandel & Mathieu 1981) they offer a rational way to seek improvements over current subgrid-scale models.

The main objective of the present study is to provide further information on the influence of the constant C_s upon the channel-flow simulations. To accomplish this we have used a well-established second-order-accurate numerical scheme with energy-conserving properties. The subgrid parametrization is of the form proposed by Smagorinsky (1963) and preferred by most authors considering flows without mean shear. The boundary conditions are similar to those used in earlier studies with coarse meshes but, owing to careful application, should give results identical with those obtained by so-called 'natural' or no-slip conditions. As the wall is approached a Prandtl mixing length is adopted, followed, at a *sufficient* resolution, by a local law-of-the-wall stress calculation.

To achieve our objectives special care must be taken with both the initial conditions and the time duration of simulations. Initial conditions of arbitrary form and large amplitude are used to provide a good chance of developing self-sustaining turbulence and a convincing demonstration of the timescales for flow adjustment. Long-term integrations for up to 45 non-dimensional time units (cf. 4 units in M & K; one unit is δ/u_τ, where δ is the channel half-separation and u_τ is the square root of the magnitude of the time-averaged surface stress) are then needed to ensure a statistically steady state and to acquire stable statistics.

In §§2.1–2.4 we describe the basic equations and the details of the numerical model. Then in §2.5 we present the parameters considered and the procedures for obtaining flow statistics. The values of C_s range from 0.07 to 0.2 and up to 51200 grid points are used. In §3 the resulting turbulence statistics and their dependence upon various parameters are examined. The conclusions are presented in §4.

2. Model description

2.1. *Basic equations*

We consider a spatially filtered velocity field $\bar{u}_i$ represented by a numerical model. Applying our unspecified-filter operation to the Navier–Stokes equations and continuity equation we have, in the high-Reynolds-number limit,

$$\frac{\partial \bar{u}_i}{\partial t}+\frac{\partial(\bar{u}_i \bar{u}_j)}{\partial x_j}=\frac{\partial \bar{P}_i}{\partial x_i}-\delta_{i1}\frac{\partial P_i}{\partial x_i}+\frac{\partial \tau_{ij}}{\partial x_j}, \tag{2.1}$$

$$\frac{\partial \bar{u}_i}{\partial x_i}=0, \tag{2.2}$$

where $(\bar{u}_1, \bar{u}_2, \bar{u}_3) \equiv (\bar{u}, \bar{v}, \bar{w})$ are the mean velocity components in the plane Poiseuille flow: u in the x-direction is the streamwise component; v in the y-direction is the component normal to the boundaries in the (x, z)-plane; and w in the z-direction is the spanwise component of flow.

A fixed streamwise mean-pressure gradient is included with the $\delta_{i1}(\partial P_i/\partial x_i)$ term, the dynamic pressure $\bar{P}_i$ includes the trace of the subgrid stress and τ_{ij} is a stress tensor. As demonstrated by Leonard (1974), in general τ_{ij} does not correspond to the usual Reynolds stresses involved in a time average. However, as noted above, in a second-order-accurate finite-difference representation τ_{ij} is consistently modelled as the usual Reynolds-stress tensor.

At this stage it is useful to make a few points concerning the finite-difference representation of (2.1). In accordance with the usual requirements for finite-difference solutions (e.g. Roache 1972), only scales of motion represented by a reasonable number of mesh points will have properties corresponding to the continuous solution. The finite-difference representations of motions on scales less than perhaps 4 grid spacings are quite unphysical. We can thus argue that a requirement for satisfactory solutions is to ensure that the stress tensor τ_{ij} provides sufficient attenuation of such scales. We should also expect that with a fixed form of stress tensor – unrelated to mesh spacing – the results should be independent of the mesh as the mesh spacing decreases. The filter function can then be regarded as defined through the fixed scale subgrid parametrization of τ_{ij} and with adequate resolution the results should be independent of the mesh and the numerical method. Indeed, if this is not the case, then the results would depend on the solution procedure and would be, to some degree, arbitrary.

Various authors (e.g. Kwak *et al.* 1975) have considered the scale of the filter function as distinct from the scale of the computational mesh. However, the view that the filter scale is determined by the subgrid parametrization, rather than *vice versa*, is new and its implications are worth discussing. They can be explained in relation to the simulation of the rate of decay of homogeneous isotropic turbulence. In any large-eddy simulation, agreement with observations should occur either when the resolved-scale motions are compared with appropriately filtered data, or when resolved plus estimated subgrid motions are compared with raw data. In previous studies of the decay of homogeneous turbulence the former approach has been used. With a Smagorinsky (1963) subgrid model and data filtered using a filter scale equal to the computational mesh the correct decay was obtained with the value of the constant $C_s \sim 0.23$. This is the value expected from theory with a filter corresponding to the mesh spacing. Rather than regard this result as a check on the determination of C_s we regard the agreement with analytic theory as an indication that the resolved-scale motions are realistic. We suggest that the decay rates simulated with

larger values of C_s seemed to give too rapid a decay only because of the comparison with data filtered at the fixed mesh scale. If as C_s was increased above 0.23 the scale of the filter applied to the data was increased proportionally we would hope that agreement would be maintained. It is not so clear that smaller values of C_s will behave in a corresponding manner. With smaller values of C_s the simulation is, in essence, being required to simulate scales smaller than the mesh spacing and errors should occur. We have not tested these ideas with simulations of homogeneous turbulence but they find support in the present study of channel flow.

2.2. *Subgrid parametrization*

The present study is not concerned with obtaining the best simulation but with understanding the role of the lengthscale implied by the subgrid model. We have thus adopted the simple, but often used, model proposed by Smagorinsky (1963). This model is the local equilibrium limit of a transport equation (Schumann 1975) to determine the subgrid-scale energy, i.e.

$$\tau_{ij} = \nu\left(\frac{\partial \bar{u}_i}{\partial x_j}+\frac{\partial \bar{u}_j}{\partial x_i}\right), \tag{2.3}$$

$$\nu = l^2(y)\,S, \tag{2.4}$$

where

$$S = \left[\frac{1}{2}\left(\frac{\partial \bar{u}_i}{\partial x_j}+\frac{\partial \bar{u}_j}{\partial x_i}\right)\left(\frac{\partial \bar{u}_i}{\partial x_j}+\frac{\partial \bar{u}_j}{\partial x_i}\right)\right], \tag{2.5}$$

and $l(y)$ is a prescribed function varying in y, the across-channel direction. The computational mesh used to resolve the y-direction has a fairly uniform value in the interior of the channel but is refined near the walls. Since there is no corresponding refinement in the spanwise and streamwise meshes there is little scope for resolving small eddies near the walls: $l(y)$ is thus not linked with mesh variations. A fixed basic value l_0 is specified and near the walls small three-dimensional eddies are represented by a Prandtl mixing-length. This in turn allows a match to the law of the wall, i.e. we require

$$l(y) \sim \kappa(y+y_0) \quad \text{as } y \to 0.$$

To link this near-wall Prandtl mixing length to the interior value we take

$$\frac{1}{l} = \frac{1}{l_0}+\frac{1}{\kappa(y+y_0)}+\frac{1}{\kappa(2\delta-y+y_0)}, \tag{2.6}$$

where κ is von Kármán's constant and $y = 0$ and $y = 2\delta$ are boundaries of the channel with midpoint $y = \delta$. y_0 is the surface roughness length for a high-Reynolds-number flow. This roughness specification arises from an intent to apply the results of this study to simulations of the planetary boundary layer. Results obtained for a boundary condition with a smooth wall are noted below.

The specification in terms of l_0 has avoided reference to the constant C_s relating l_0 to the typical mesh spacing. To provide comparisons with previous work in terms of values of C_s we define

$$C_s = \frac{l_0}{(\Delta x\,\Delta y_{\max}\,\Delta z)^{\frac{1}{3}}}, \tag{2.7}$$

where Δx and Δz are the constant grid intervals in the streamwise and spanwise directions respectively and $\Delta y_{\max}$ represents the maximum (in practice a typical value) grid interval across the channel.

From the above comments on numerical solutions, the flows obtained for fixed l_0 and varying numerical resolution should only differ in consequence of finite-difference errors. C_s can be regarded as a measure of the finite-difference resolution. For a fixed numerical mesh the value of C_s giving the best results is likely to be a compromise. Low values of C_s resolve the greatest range of scales but have potential finite-difference errors. High values of C_s give a limited range of scales but offer good finite-difference solutions. The derivations of C_s from inertial-subrange arguments (Lilly 1967) are likely to be a sensible compromise as they correspond to a small amount of energy on mesh scales. Obtaining the correct decay rate for homogeneous turbulence (e.g. Antonopoulos-Domis 1981) has provided a convincing test that this choice is satisfactory.

2.3. *Boundary conditions*

Equation (2.2) is solved in the three-dimensional domain $(0, L), (0, W), (0, 2\delta)$, where L and W are the length and span of the domain. These are selected in accord with previous studies (M & K) and the choice is discussed below. In the streamwise and spanwise directions the domain is assumed periodic, i.e.

$$f(x+L) = f(x), \quad f(z+W) = f(z)$$

for all variables.

Normal to the channel walls we enforce the local law-of-the-wall relation for high-Reynolds-number flow over a rough surface (see Townsend 1976, p. 140, but note the change in the definition of the value of y at which $u = 0$), i.e.

$$\bar{u}_A = \frac{u_*}{\kappa} \cos\theta \ln\left(1+\frac{\Delta_A}{y_0}\right), \quad \bar{w}_A = \frac{u_*}{\kappa} \sin\theta \ln\left(1+\frac{\Delta_A}{y_0}\right), \tag{2.8}$$

where $(\bar{u}_A, \bar{w}_A)$ are the velocity components in the (x, z)-directions at the lowest grid point a distance $y = \Delta_A$ from the wall, i.e.

$$u_*^2 = \frac{1}{M} |\boldsymbol{v}_A| \cdot \boldsymbol{v}_A,$$

where $1/M = (1/\kappa^2) \ln^2(1+\Delta_A/y_0)$ and $\boldsymbol{v}_A$ is the vector velocity at the lowest grid point. These relationships are used to calculate the local values of instantaneous surface stress $u_*^2 \cos\theta$, $u_*^2 \sin\theta$ in the (x, z)-directions.

To apply such a boundary condition, flow acceleration at $y = \Delta_A$ must be negligible and steady statistics expected. When the flow acceleration is small the solutions close to the wall amount to local 'constant-stress' boundary-layer solutions and the near-wall Prandtl mixing length corresponds exactly to the local law of the wall. The flow accelerations are of order τ_0/δ and in the present study we find peak values (essentially $\partial\bar{p}/\partial x$) $\approx 5\tau_0/\delta$. To neglect such accelerations Δ_A must be much less than 0.2δ; this is well satisfied here with $\Delta_A \approx 0.005\,\delta$. The validity of this approach was confirmed by demonstrating that the solutions do not depend on the mesh resolution Δ_A.

In the flow interior τ_{ij} is assumed, incorrectly, to have a deterministic relationship with the deformation S, and it is not consistent to consider the possibility of a statistical variation in the boundary condition. In fact, owing to the small values of $l^3(y)/\Delta_A \Delta_x \Delta_z$, the calculations of the surface values of τ_{ij} represent an average over a volume much greater than the scale of the turbulence ($\approx \Delta_A^3$). These are arguably the only values of τ_{ij} which are correctly assumed to be deterministic.

In common with all flows with multiple timescales a particular law-of-the-wall

relation cannot be satisfied on more than one timescale (Townsend 1976, p. 156). This is not only a feature of the application of a law of the wall but also of Prandtl-mixing-length solutions. In the present case the time-mean flow satisfies

$$\langle \bar{u}_A(\bar{u}_A^2+\bar{w}_A^2)^{\frac{1}{2}}\rangle_t = u_\tau^2 \ln^2\left(1+\frac{\Delta_A}{y_0}\right), \tag{2.9}$$

where $\langle\ \rangle_t$ denotes time average. The departure of the time-mean flow from the law of the wall depends on the ratio of the resolved-scale variance to the mean flow at $y = \Delta_A$ and in the present study

$$\frac{\langle \bar{u}_A(\bar{u}_A^2+\bar{w}_A^2)^{\frac{1}{2}}\rangle_t - \langle \bar{u}_A\rangle_t^2}{\langle \bar{u}_A(\bar{u}_A^2+\bar{w}_A^2)^{\frac{1}{2}}\rangle_t}$$

is about 0.05. Owing to the nonlinear character of the law of the wall such behaviour is inevitable in calculations and observational data. It is a simple consequence of the presence of scales of motion other than those involved in the local wall equilibrium.

The procedure adopted here can easily be applied to high-Reynolds-number flow over a smooth wall. In this case

$$\boldsymbol{v}_A \cdot |\boldsymbol{v}_A| = u_*^2\left(\frac{1}{\kappa}\ln\frac{u_*\Delta_A}{\nu_{\mathrm{M}}}+C_{\mathrm{w}}\right)^2, \tag{2.10}$$

where ν_{M} is the kinematic viscosity and C_{w} an empirical constant of value about 5.0. This boundary condition was implemented through an iterative procedure involving refinement of an initial guess for u_*. A test integration with ν_{M} taking a value such so that $\nu_{\mathrm{M}}/u_\tau = 10^{-3}\delta$ (the value of y_0 considered) gave very similar results to those obtained with the rough-surface boundary conditions (2.8). The only significant difference was an increase in mean flow speeds of about $5.0u_\tau$; this resulted from the 'slip' of $C_{\mathrm{w}}u_*$ implied by (2.10). As discussed by Townsend (1976, p. 135) this implied flow similarity of high-Reynolds-number flow over smooth and rough walls is to be expected.

2.4. *Numerical methods*

The numerical procedure follows well-established methods whose performance has been well documented. The variables are stored on the usual staggered mesh as in Williams (1969). In order to avoid averaging of the important y-derivatives of the mean flow the values of S and eddy-viscosity ν are evaluated and stored upon v-points. To calculate S the individual stresses τ_{ij} are calculated on the particular grid-point locations at which they are used in the momentum equations. These values are then squared and S is derived by averaging the squares onto the v-points. This averaging procedure ensures that the volume-averaged dissipation is equal to the volume average of νS^2. The mesh stretching in the y-direction occurs smoothly and does not compromise the second-order-accurate spatial derivative (Kalnay de Rivas 1972). The inertial terms are calculated using the 'absolutely conserving' scheme of Piacsek & Williams (1970) and are time-advanced by a leap-frog scheme. A weak time filter (Mason & Sykes 1978) is applied continuously to prevent time-splitting. The viscous terms are calculated with a simple forward step. Owing to the moderate 'turbulent' Reynolds number characterizing the flows this does not give a loss of accuracy and was adopted to avoid the complexities of coding and storage organization associated with implicit methods. The stability of the forward step imposed a limit to the mesh refinement. In the examples considered, the mesh refinement has been selected so that the Courant condition ((2.11) below) remains more restrictive than the viscous

δ = channel half-width	Domain length $L = 6\delta$
y_0 = surface-roughness length	Domain width $W = 3\delta$
u_τ = square root of surface stress	$y_0/\delta = 10^{-3}$
u_c = centreplane velocity	$u_c/u_\tau \approx 22$

TABLE 1. Basic parameters

Run no.	N_x	N_y	N_z	$\frac{\Delta x}{\delta}$	$\max\frac{\Delta y}{\delta}$	$\frac{\Delta z}{\delta}$	C_s	$\frac{l_0}{\delta}$	Averaging time
A2	40	40	32	0.15	0.066	0.094	0.2	0.019	12
B2	20	26	16	0.3	0.124	0.188	0.2	0.038	11
B1	20	26	16	0.3	0.124	0.188	0.1	0.019	12
C2	16	18	12	0.375	0.229	0.25	0.2	0.056	1
C1	16	18	12	0.375	0.229	0.25	0.1	0.028	13
C07	16	18	12	0.375	0.229	0.25	0.07	0.019	12
D1	10	18	8	0.6	0.229	0.375	0.1	0.037	13

TABLE 2. Details of the numerical simulations. Ni is the number of grid points in the i-direction, Δi is the corresponding grid interval and the averaging time is in units of δ/u_τ.

criterion (2.12). The Poisson equation for pressure is solved by a direct method using a fast Fourier transformation in the directions parallel to the channel walls and a line inversion of the resulting tridiagonal matrices normal to the walls. With a mesh of $40 \times 40 \times 32$ grid points each time step of the model takes about 8 s CPU time on an IBM 3081.

2.5. *Parameters and procedures*

The relative dimensions of the computational domain (table 1) were selected in accord with previous large-eddy simulations and ensure that the dominant scales determined in the experimental data of Comte-Bellot (1963) are included. Owing to the consideration of high-Reynolds-number flow over a rough surface, the channel flow depends on the parameter y_0/δ, which in all cases was taken to be 10^{-3}. If the molecular-viscosity term is small or, as in the present study, zero then similarity considerations can be applied. The flow in the interior of the channel will be a fixed function of u_τ and δ and only the wall relations will depend upon either y_0 or, if a smooth wall, the Reynolds number. The flow in the centre of the channel will be given by either

$$\frac{u_c}{u_\tau} = u_{c0} + \frac{1}{\kappa}\ln\left(\frac{\delta}{y_0}\right)$$

or

$$\frac{u_c}{u_\tau} = u_{c0} + \frac{1}{\kappa}\ln\left(\frac{u_*\delta}{\nu_M}\right) + C_w,$$

depending on whether the wall is rough or smooth. Here u_{c0} is a constant for high-Reynolds-number channel flow. In the present study, apart from these changes in the 'origin' of the mean-flow profiles there should thus be no other dependence upon Reynolds number or y_0. The maximum number of grid points used was 51200 and table 2 summarizes the number of mesh points and other characteristics of each

	Mesh A		Mesh B		Mesh C and D	
n	y	Δy	y	Δy	y	Δy
1	0.000	—	0.000	—	0.000	—
2	0.0036	0.0036	0.0058	0.0058	0.0104	0.0104
3	0.0127	0.0091	0.0209	0.0151	0.0384	0.0280
4	0.0273	0.0146	0.0465	0.0256	0.0876	0.0492
5	0.0507	0.0234	0.0889	0.0424	0.1708	0.0832
6	0.0850	0.0343	0.1521	0.0632	0.2958	0.1250
7	0.1301	0.0451	0.2360	0.0839	0.4626	0.1668
8	0.1843	0.0542	0.3371	0.1011	0.6633	0.2007
9	0.2445	0.0602	0.4498	0.1127	0.8854	0.2221
10	0.3081	0.0636	0.5690	0.1192	1.1146	0.2292
11	0.3733	0.0652	0.6912	0.1222		
12	0.4391	0.0658	0.8145	0.1233		
13	0.5050	0.0659	0.9381	0.1236		
14	0.5710	0.0660	1.0618	0.1237		
15	0.6370	0.0660				
16	0.7030	0.0660				
17	0.7690	0.0660				
18	0.8350	0.0660				
19	0.9010	0.0660				
20	0.9670	0.0660				
21	1.0330	0.0660				

TABLE 3. Grid distribution in the y-direction from the wall to the centre of the channel. n is the grid-point number, y the normalized distance from the wall and Δy the local mesh spacing.

simulation. The meshes used in the y-direction are derived by smoothing a mesh consisting of linear sections, and the three meshes used are presented in table 3.

In keeping with results reported in the literature, the ability of the model to sustain resolved turbulent fluctuations was found to depend upon the initial conditions. To develop self-sustaining turbulence it was found essential to start with an excessive value of centreline velocity. The initial mean-velocity profile was thus taken as the equilibrium-velocity profile occurring in the absence of resolved-scale motions. This 'mixing-length' solution was calculated using the finite-difference mesh and the chosen value of l_0. The initial flow perturbation consisted of an alternating addition and subtraction of a velocity u_c, from cubic blocks of fluid of size δ^3. This preserved the mean-velocity profile but was quite arbitrary.

This arbitrary initialization procedure forces the use of integration periods sufficient to give statistically steady results. The surface stress on the channel took about $20\,\delta/u_\tau$ to assume its steady-state value and model statistics were not obtained until after $25\,\delta/u_\tau$. It is clear that some previous studies over periods of $\approx 4\,\delta/u_\tau$ were highly dependent on initial conditions and might, given longer timescales, have shown further changes. The present turbulent statistics were obtained by averaging results sampled at intervals of $0.01\,\delta/u_\tau$ over a period of $\approx 10\,\delta/u_\tau$. Although shorter periods $\approx \delta/u_\tau$ gave similar statistics this longer period was necessary to make the statistics symmetric (within a few percent accuracy) about the centre of the channel. During the integrations the quantities

$$C_1 = \max\left[\left|\frac{2\Delta t\,\bar{u}}{\Delta x}\right|, \left|\frac{2\Delta t\,\bar{v}}{\Delta y(y)}\right|, \left|\frac{2\Delta t\,\bar{w}}{\Delta z}\right|\right] \tag{2.11}$$

and
$$C_2 = \max\left[\frac{8\nu\,\Delta t}{\min\left(\Delta x^2, \Delta y^2(y), \Delta z^2\right)}\right], \tag{2.12}$$

where Δt is the time step, were both kept less than 0.3 and the larger of two usually greater than 0.2. This was achieved by reviewing the value of Δt at intervals of $0.1\,\delta/u_\tau$. To minimize C_1 the equations were subject to a Galilean transformation which was also reviewed at intervals of $0.1\,\delta/u_\tau$.

In what follows we will use angular brackets $\langle\ \rangle$ to denote variables averaged in time and (x, z)-planes parallel to walls. The variable u' is defined as the departure of $\bar{u}$ from its instantaneous (x, z)-plane average. The off-diagonal subgrid-stress components of τ_{ij} are calculated from (2.3) whilst the diagonal values τ_{ii} have an isotropic constant $\frac{2}{3}k$ added. In accord with the mixing-length limit of high-order closure techniques (Launder & Spalding 1972), k is given by

$$k = C_E^{-1}\, l^2(y)\, S^2,$$

where C_E is a constant stress-energy ratio assumed to have the value 0.3. This simple diagnostic model of subgrid turbulence energy is only intended to give an appraisal of the general magnitude of the subgrid energy. At the channel wall it implies an unrealistic isotropy of the energy components. Except for the present simple objectives it would be better to use an anisotropic parametrization in the region near the walls.

3. Results

As already noted the parameters characterizing each of the flow simulations are summarized in table 2. Each simulation is denoted by a letter followed by a number. The letter indicates the mesh used and the number the value of C_s. The values of C_s and l_0 have been varied independently, e.g. runs A2, B2 and C2 all have $C_s = 0.2$ but have different values of l_0 whilst runs A2, B1 and C07 have the same value of l_0.

In previous work, where a value was assigned to C_s, a value of l_0 could be calculated from the typical mesh spacing. The smallest value of l_0 used here, $l_0 = 0.019\delta$, is similar to the values of 0.018δ and 0.013δ used in the studies of Moin *et al.* (1978) and Deardorff (1970) respectively. In the study of M & K a much finer mesh was used and l_0 had the value 0.005δ.

In view of the apparent difficulties of some previous studies in sustaining resolved-scale turbulence it is convenient to begin with an examination of the statistics for $\bar{v}$. Figure 1 (*a*) illustrates the time history of the grid-point-averaged value of $\bar{v}^2$. Owing to the non-uniform grid spacing near the walls, this value is very slightly smaller than the volume-averaged value of $\bar{v}^2$. The three cases presented (A2, B2 and C2) are typical of the types of behaviour observed. In each case the initial high amplitude decays quickly and near-equilibrium is achieved at $t \approx 20\delta/u_\tau$. Long-term $\approx 10\,\delta/u_\tau$ fluctuations are evident in the cases with sustained energy. Run B1 is not shown but is similar to A2. Run B2 shows a low level of sustained energy. An earlier attempt to generate run B2 by changing the value of l_0 in run B1 at time $25\,\delta/u_\tau$ gave no resolved-scale motions and illustrated the importance of initial conditions. Run C2 shows no sustained resolved-scale motions. These results suggest that with an adequate mesh (A) the value of C_s found favourable for homogeneous turbulence will allow a sensible channel-flow simulation.

These long-term fluctuations in the turbulence energy are related to fluctuations in the space-average stress on the walls of the channel. Figure 1 (*b*) shows the time

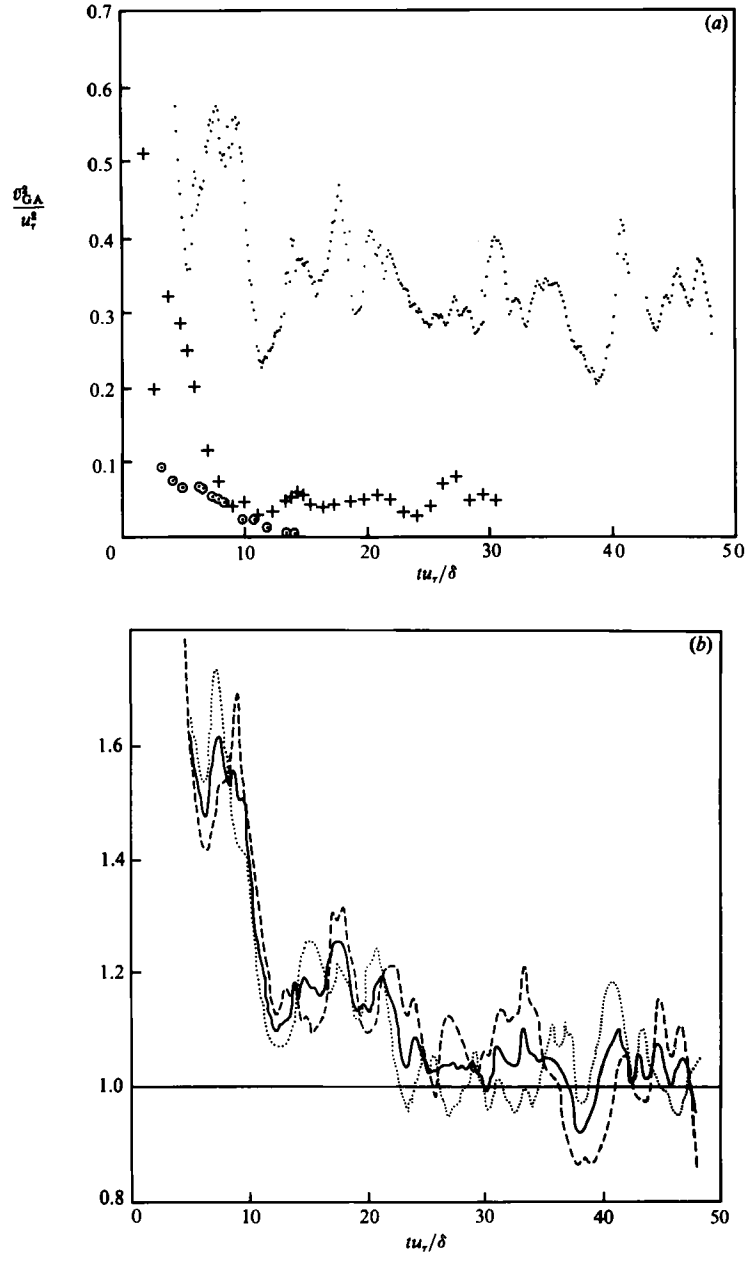

FIGURE 1. The time evolution of statistics. (*a*) The evolution of the variance of $\bar{v}$ averaged over the total number of grid points in the whole computational domain, $\bar{v}^2_{\mathrm{GA}}$. Results for cases A2 (.....), B2 (+) and C2 (⊙) are given and each symbol denotes a successive time average. As indicated by the symbol spacing, the averaging periods varied between cases. (*b*) The evolution of the space-average wall stress for case A2. The stress on each wall and the net stress are shown separately. Values are derived as time averages over the same intervals as used in (*a*). For ease of presentation continuous curves have been drawn: – – –, wall stress $y = 2\delta$; ....., wall stress $y = 0$; ——, mean wall stress.

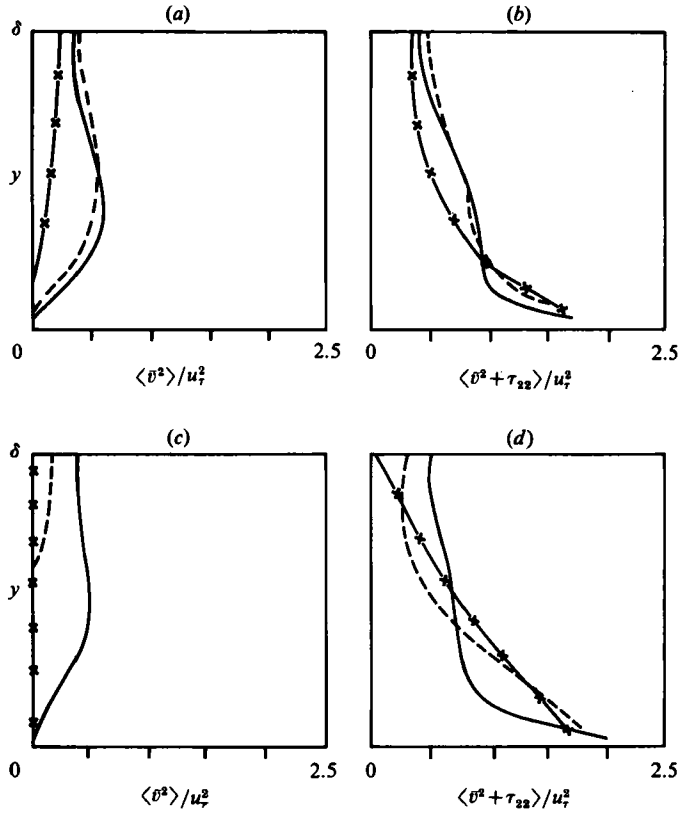

FIGURE 2. Profiles of the y-variation of the resolved $\langle \bar{v}^2 \rangle$ and total $\langle \bar{v}^2 + \tau_{22} \rangle$ variance. (*a*) and (*b*) $C_s = 0.1$. ——, B1; – – –, C1; ×—×, D1; (*c*) and (*d*) $C_s = 0.2$. ——, A2; – – –, B2; ×—×, C2.

evolution of the wall stress for case A2. The stress on each of the walls and the net wall stress are illustrated. It is evident that after about $25\,\delta/u_\tau$ the fluctuations are of order 10% of the time mean and mask any longer-term tendencies. The average statistics presented below were obtained over the last period of duration $10\,\delta/u_\tau$. During this period the wall stress is a few percent above the long-term time mean determined by the basic pressure gradient. This departure from the long-term mean may be a combination of incomplete adjustment to equilibrium or a statistical fluctuation. Comparison of average statistics obtained from successive intervals of duration $10\,\delta/u_\tau$ suggest a statistical error of a few percent for the results given below. The asymmetrics between the stress on the walls have a bigger amplitude than the variation in the mean, and differences of 20% of time-mean value persist for several δ/u_τ. Both the asymmetries and time variations indicate that boundary conditions that assume a fixed value of wall stress will be unrealistic.

Figure 2 illustrates the profiles of resolved and total $\bar{v}$-variance normal to the channel walls, i.e. $\langle \bar{v}^2 \rangle$ and $\langle \bar{v}^2 + \tau_{22} \rangle$ respectively. Owing to the near-symmetry about the centre of the channel only one half of the profile is shown. The cases are grouped into fixed values of C_s with varying mesh resolution. The cases with $C_s = 0.2$ are the ones whose time dependence is illustrated in figure 1. The total variance in cases B2 and C2 are dominated by τ_{22} and tend towards a linear variation corresponding to the fixed subgrid-stress-energy ratio. With $C_s = 0.1$ cases B1 and C1 both give

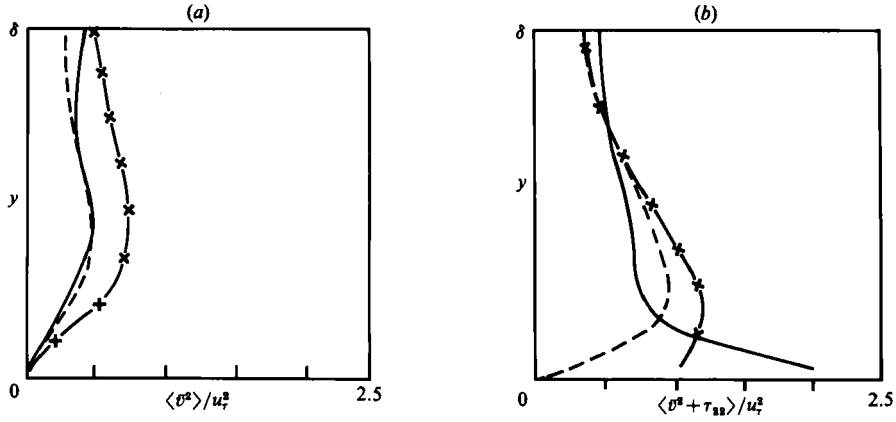

FIGURE 3. Profiles of the y-variation of the $\bar{v}$ variance. (a) The resolved-scale $\langle\bar{v}^2\rangle$ for three cases with $l_0 = 0.019\delta$: ——, A2; – – –, B1; × — ×, C07. (b) The total variance $\langle\bar{v}^2+\tau_{22}\rangle$ for case A2 (——) compared with the simulation of Moin & Kim (1982) (– – –) and the observations of Comte-Bellot (1963) (× — ×).

realistic resolved-scale motions but there are weaker eddies in case D1. These results show that as C_s is reduced from 0.2 to 0.1 a coarser mesh will support resolved-scale turbulence.

In figure 3(a), the profiles of v-variance are grouped together for a constant value of $l_0/\delta = 0.019$. The curves for A2 and B1 have already been shown and C07 is included. In contrast to the large changes in resolved-scale motion with fixed C_s and varying resolution the changes with l_0 fixed are less marked. There remains a tendency for the values of $\langle\bar{v}^2\rangle$ to increase as the numerical resolution decreases. Since the basic continuous equations posed for these cases are the same, we argue that the changes must be attributed to finite-difference errors. Although a run with better resolution than mesh A has not been conducted we expect finite-difference errors to be small in case A2. We discuss this point further below when examining the velocity fields.

For comparison, in figure 3(b), curves of resolved $\bar{v}$-variances from the simulation of M & K and the experimental data of Comte-Bellot (1963) are shown. These results are for Reynolds numbers (based on centreplane flow speed) of 13800 and 57000 respectively but provide the best available comparisons. We should emphasize that we have not sought to conduct the best simulation but rather to understand the role of C_s and l_0. The M & K results are obtained with a smaller value of l_0 and, especially near the wall, a larger resolved component is expected. When compared with the experimental data the present case A2 shows fair agreement but not as good as that obtained by M & K. In particular it is evident that close to the wall the subgrid variance is excessive. This is only a diagnostic consequence of the assumed isotropy of the subgrid variance and is not inherent in the calculation.

Profiles of $\bar{u}$- and $\bar{w}$-variance are shown in figures 4 and 5. With $\bar{u}$ the coarser-resolution results B1 and C07 show less variance than case A2. This seems to be associated with the more-marked longitudinal structures in case A2. The values of $\langle(u)^2+\tau_{11}\rangle$ are somewhat greater than those observed or those obtained by M & K. With w the values of variance are somewhat less than observations and the results of M & K. We feel the discrepancies are best attributed to the limited range of resolved scales in the present study and would hope that with more mesh points better results could be obtained. It seems that in the present simulations with $l_0 = 0.019\delta$ the

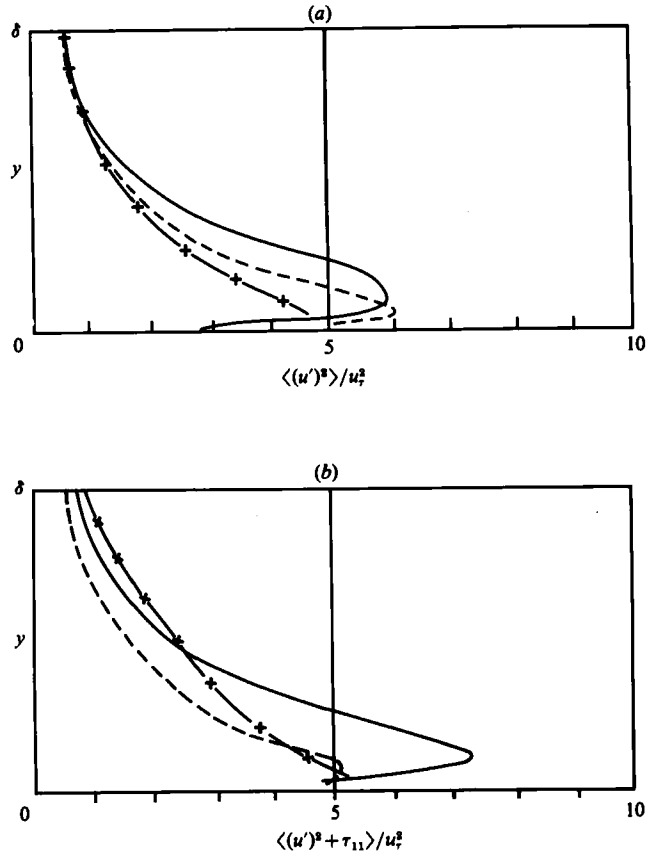

FIGURE 4. Profiles of the y-variation of the streamwise-velocity-component variance. (*a*) The resolved-scale $\langle(u')^2\rangle$ for three cases with $l_0 = 0.019\delta$: ——, A2; – – –, B1; × — ×, C07. (*b*) The total variance $\langle(u')^2+\tau_{11}\rangle$ for case A2 (——) compared with the simulations of Moin & Kim (1982) (– – –) and the observations of Comte-Bellot (1963) (× — ×).

organized longitudinal structures are too important. A smaller value of l_0, as used by M & K, will allow a higher 'eddy-viscosity Reynolds number' and more scope for introducing a higher degree of random structure.

Figure 6 shows profiles of stress $\langle\bar{u}\bar{v}+\tau_{12}\rangle$ and $\langle\bar{u}\bar{v}\rangle$ across the whole channel for case A2. The significance of the subgrid scale is well illustrated and a minor asymmetry is evident in the non-zero value of stress at $y = \delta$. This is a feature of the finite averaging period and is precisely related to asymmetries in the mean-velocity profiles. The mean-velocity profiles (figure 7) show maximum values which vary nearly inversely with the resolved-scale $\bar{v}$-energy. The velocity profiles for cases B1 and A2 are illustrated and are fairly similar. The velocity profile for case B2 is essentially a mixing-length solution based on the scale l_0. It shows a greater velocity but is not grossly unrealistic. Values of l_0 equal to 0.05δ give realistic values of centreline velocity. It should thus come as no surprise that values of l_0 of about $0.04\,\delta$ and greater give no resolved-scale motions. The subgrid parametrization is then a crude but adequate representation of the turbulent flow. For comparison the experimental data of Hussain & Reynolds (1975) and Comte-Bellot (1963) at Reynolds numbers of 13800 and 57000 respectively are illustrated. The comparison

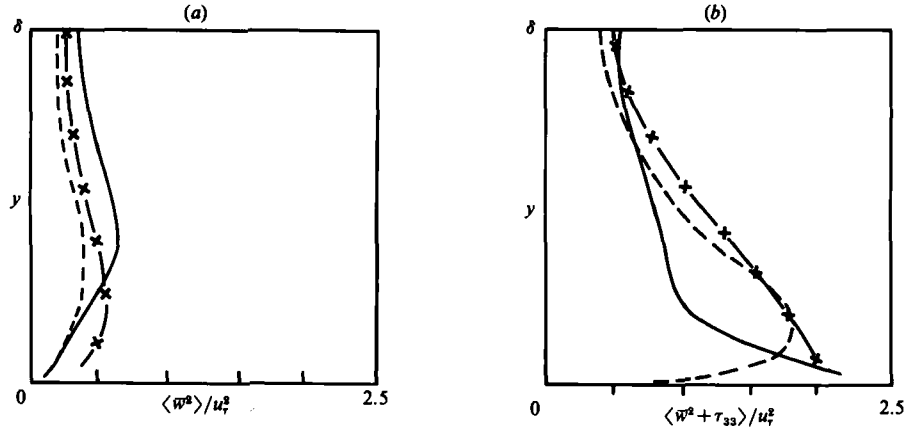

FIGURE 5. Profiles of the y-variation of the spanwise-velocity-component variance. (a) The resolved-scale $\langle \bar{w}^2 \rangle$ for three cases with $l_0 = 0.019\delta$: ——, A2; – – –, B1; × — ×, C07. (b) The total variance $\langle \bar{w}^2 + \tau_{33} \rangle$ for case A2 (——) compared with the simulation of Moin & Kim (1982) (– – –) and the observations of Comte-Bellot (1963) (× — ×).

is confounded by both the difference between smooth- and rough-wall boundary conditions and the different values of Reynolds number. When the profiles are shifted so that the velocities near the wall agree there is good agreement.

As noted by M & K the correlation coefficient for the shear stress

$$C_{12} = \frac{\langle \bar{u}\bar{v} + \tau_{12} \rangle}{(\langle (u')^2 + \tau_{11} \rangle \langle \bar{v}^2 + \tau_{22} \rangle)^{\frac{1}{2}}}$$

should provide an indication of the realism of the resolved-scale motions. In figure 8 this coefficient is compared with the experimental data of Sabot & Comte-Bellot (1976). The agreement is particularly good and very similar to that found by M & K in their simulations.

We conclude our presentation of results with an examination of sections of the flow field. Figure 9 illustrates sections in a plane parallel to the channel walls at $y = \frac{1}{12}\delta$. Fields of the velocity component normal to wall $\bar{v}$ are given for runs A2, B1 and C07, i.e. a constant value of $l_0 = 0.019\delta$. In case A2 (figure 9a) the field shows some evidence for the characteristic streak structure seen in previous studies (M & K) and observations (Runstodler, Kline & Reynolds 1963). These streaks can be seen clearly in the $\bar{u}$-field discussed below. The distribution of mesh points is indicated at the edge of the frame and it is evident that the structures are smoothly described and well represented. In case B1 (figure 9b) the streaks are much less pronounced and the field is similar to that seen at greater values of y (see below). The numerical representation is not as good as it should be, with a number of significant features dominated by single grid-point values. The contour-plotting routine uses simple linear interpolation and provides a faithful representation of the grid-point values. Case C07 (figure 9c) has very poor resolution and the structures are quite unphysical. The fact that case C07 gives plausible turbulence statistics should strike more a note of caution than a declaration of success. With such a poor description of the flow and obvious severe finite-difference errors there can be little correspondence with the Navier–Stokes equations.

The inadequacy of the finite-difference representation used in cases C07 and B1 is confirmed by the form of the spatial spectra of the velocity components. Figure 10

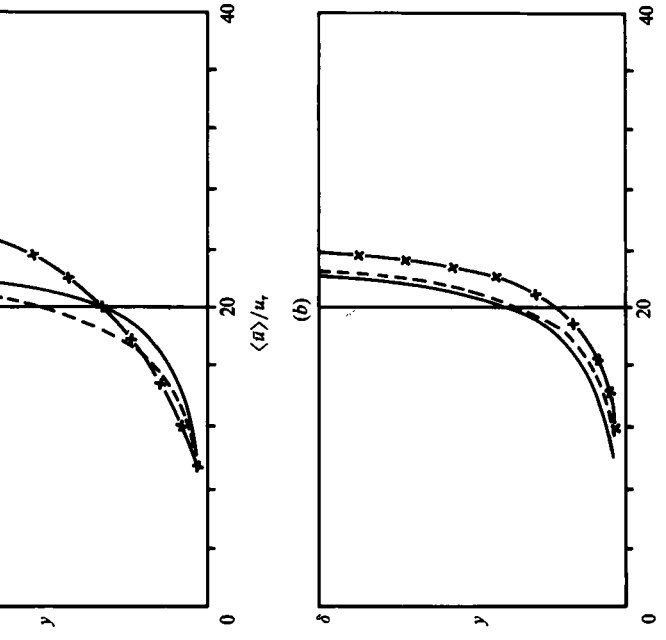

FIGURE 7

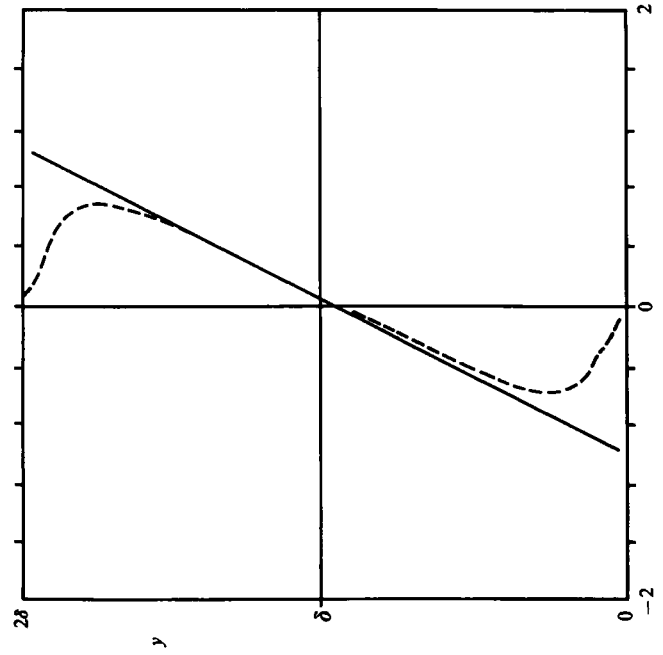

FIGURE 6

FIGURE 6. Profile of the y-variation of the total $\langle \bar{u}\bar{v}+\tau_{12}\rangle$ and resolved $\langle \bar{u}\bar{v}\rangle$ stress for run A2.

FIGURE 7. Profile of the y-variation of the mean-velocity profile $\langle \bar{u}\rangle$. (*a*) Profiles for cases A2 (——), B1 (– – –) and B2 (×—×). (*b*) The A2 profile (——) compared with observations of Hussein & Reynolds (1975) (– – –) and Comte-Bellot (1963) (×—×).

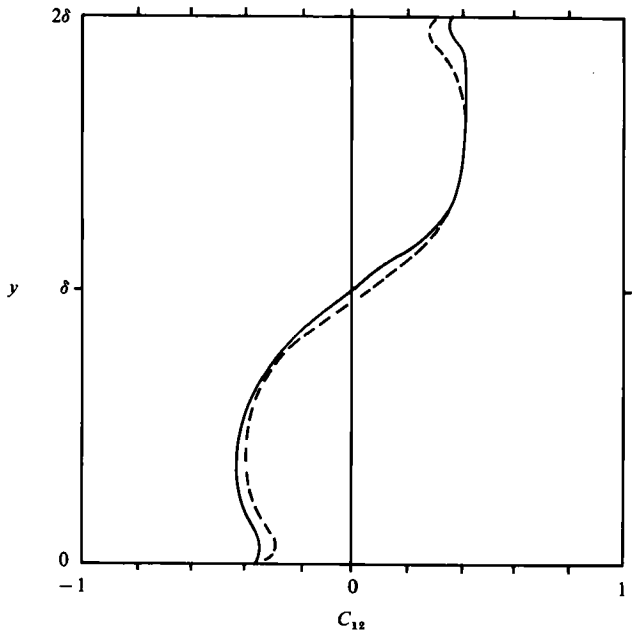

FIGURE 8. Profile of the y-variation of the correlation coefficient

$$C_{12} = \frac{\langle \bar{u}\bar{v} + \tau_{12} \rangle}{(\langle (u')^2 + \tau_{11} \rangle \langle \bar{v}^2 + \tau_{22} \rangle)^{\frac{1}{2}}}$$

for case A2. The solid curve shows the experimental data of Sabot & Comte-Bellot (1976).

shows x-direction spectra of the v-component of flow. In accord with the profiles of $\langle \bar{v}^2 \rangle$ the energy density in low wavenumbers is seen to increase as the resolution decreases. At the same time the energy density on the shortest scales also increases. In contrast to the other cases, in A2 it is seen that on scales shorter than $4\,\Delta x$ ($m = 10$) there is a rapid fall of energy density with increasing wavenumber.

A more detailed examination of the flow fields in case A2 confirms their plausible appearance. Figures 11 (*a*) and (*b*) show the sections of streamwise $\bar{u}$- and spanwise $\bar{w}$-velocity components at $y = \frac{1}{12}\delta$ corresponding to the realization of $\bar{v}$ given in figure 9 (*a*). The spanwise component can be largely accounted for by the continuity of flow in two-dimensional flow streaks. A comparison of the streamwise and $\bar{v}$-components shows a negative correlation between $\bar{u}$ and $\bar{v}$ which corresponds to the transfer of momentum towards the walls.

Figure 12 shows a section of the $\bar{v}$-field in a plane parallel to channel walls at $y = \frac{1}{2}\delta$. The streaks are less evident and the turbulent eddies near the centre of the channel have a more isotropic structure. Sections in the (z, y)-plane normal to the stream are shown in figures 13 (*a*) and (*b*). The y-direction scale allows an equal distance for each mesh point and true values of y can be deduced from values on the axis of the diagrams. Figure 13 (*a*) shows contours of the streamwise flow and figure 13 (*b*) shows flow vectors in the (z, y)-plane. Near the walls the high correlation between $\bar{u}$ and $\bar{v}$ is again clearly evident. The resolved eddies are well represented by the finite-difference mesh. The parametrization of near-wall turbulence with $l_0 \approx \kappa(y + y_0)$ occurs below a height $\approx 0.05\delta$ where it is clear that small-scale three-dimensional motions could not be represented.

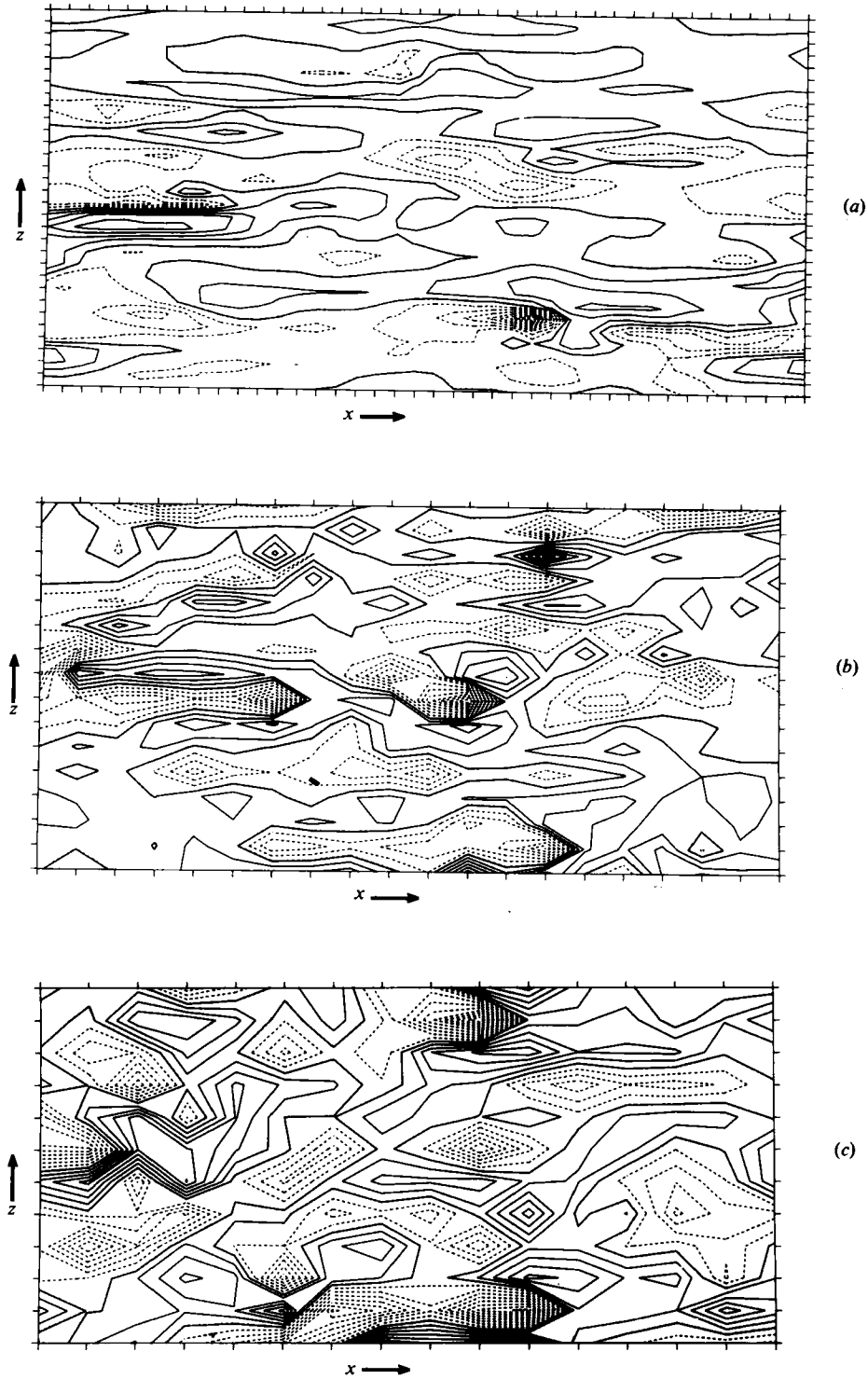

FIGURE 9. Section of the $\bar{v}$-velocity fields in the (x, z)-plane at $y = \frac{1}{12}\delta$. (*a*), (*b*) and (*c*) illustrate results from cases A2, B1 and C07 (constant $l_0 = 0.019\delta$) respectively. Negative values are denoted by dashed contours and the contour intervals are $0.126u_\tau$, $0.175u_\tau$ and $0.148u_\tau$ respectively.

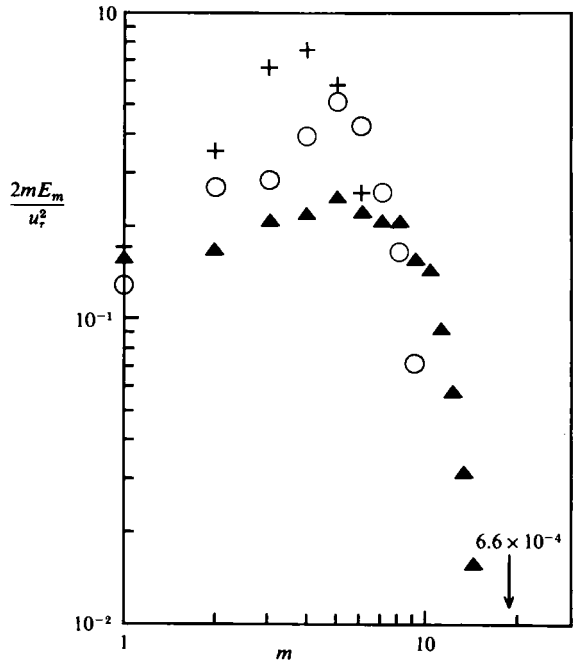

FIGURE 10. Spectra of v for cases A2 (▲), B1 (○) and C07 (+). Time and spanwise average of the x-direction spectra of v in the centre of the channel. The wavenumbers m are given by $m = L/\lambda$, where λ is the wavelength. E_m is the energy in each wavenumber.

4. Conclusions

A series of large-eddy simulations of plane Poiseuille flow have been conducted. In the interior of the flow the subgrid-scale motions are parametrized with the eddy-viscosity formulation proposed by Smagorinsky (1963). Near the walls this is matched to a Prandtl-mixing-length solution. The lengthscale used in the Smagorinsky formulation l_0 is related to a typical mesh spacing Δ by the usual constant $C_s = l_0/\Delta$.

The resolved-scale turbulence energy in the simulations is found to depend primarily upon the value of l_0/δ, where δ is the channel half-width. Values of $l_0/\delta \gtrsim 0.05$ give no resolved-scale eddies and only when l_0 is less than $\approx 0.03\delta$ do resolved-scale eddies seem sustainable. In fact, unless initial conditions are carefully chosen l_0 must be less than $0.02\,\delta$ for sustained eddies.

If C_s is varied with constant mesh spacing Δ then l_0 is also varied and the results show a strong dependence on C_s. However, if C_s is varied by changing the mesh spacing with l_0 held fixed, the variations are much weaker. It is also evident that, whilst larger values of C_s (≈ 0.2) give flows with a smoothly varying spatial structure, smaller values of C_s (≈ 0.1) give flows with excessive amounts of grid-scale motions. This result was anticipated from general considerations of numerical methods. The smaller values of C_s thus appear to give excessive finite-difference departures from the continuous solutions. Large values of C_s give smooth solutions but, if too large, waste numerical resources. The value of C_s found consistent with the cascade of energy in homogeneous isotropic turbulence, ≈ 0.2, seems close to optimum and gives solutions with just adequate numerical resolution.

The previous suggestion (Deardorff 1970*a*) that the simulation of shear-driven turbulence requires a smaller value of C_s than homogeneous isotropic turbulence is

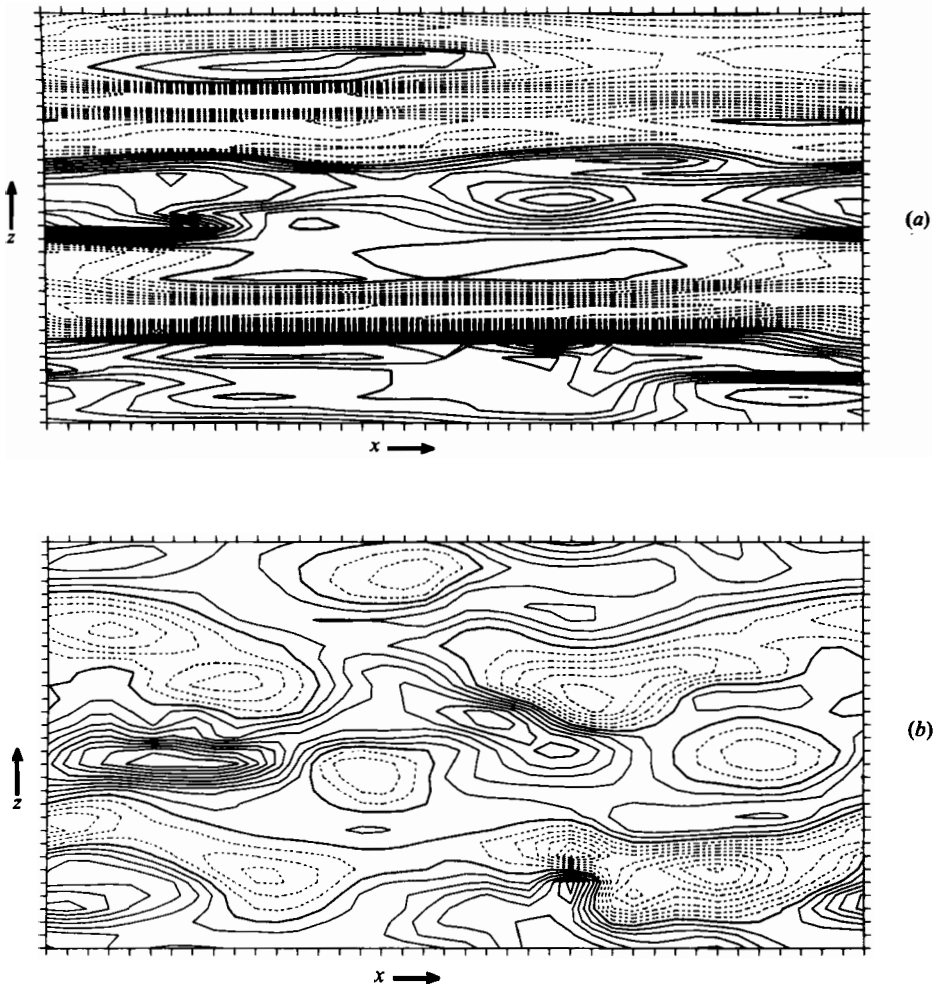

FIGURE 11. Sections of the $\bar{u}$ (figure 10*a*) and $\bar{w}$ (figure 10*b*) velocity fields in the (x, z)-plane at $y = \frac{1}{12}\delta$ for case A2 for the same time as the $\bar{v}$-field shown in figure 9(*a*). Negative values are denoted by dashed contours and the contour intervals are $0.469u_\tau$ and $0.128u_\tau$ respectively.

not verified. Provided $l_0 \lesssim 0.02\delta$, simulations with $C_s = 0.2$ appear quite satisfactory. The ratio of l_0 to the scale of the flow δ is a measure of the 'turbulent'-eddy-viscosity-based Reynolds number of the flow and unless l_0 is $\lesssim 0.02\delta$ this Reynolds number is simply too low for sustained eddies. In fact when l_0 is $\gtrsim 0.05\delta$ the velocity profile determined by the subgrid stresses has a maximum value less than that observed and there is no requirement for further transport processes.

In addition to considering the role of the parameters l/δ and C_s, the present study has provided further examples of large-eddy simulations. The turbulent statistics obtained in the present study with $l_0 = 0.019\delta$ and $C_s = 0.2$, like those of previous studies, are most encouraging. A new result obtained through the use of much longer-duration simulations is an identification of the timescales for flow adjustment and the presence of long-timescale fluctuations. A timescale of $\approx 20\delta/u_\tau$ (where u_τ is the square root of the surface stress) is needed to obtain a correct flow independent

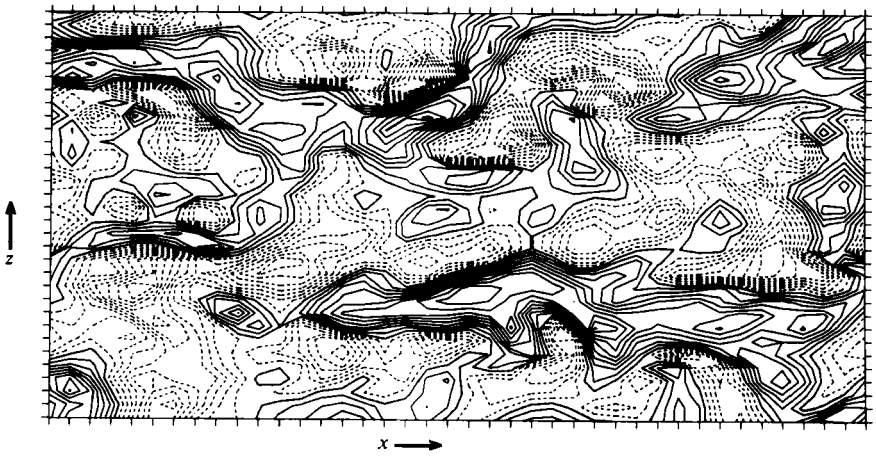

FIGURE 12. Section of the $\bar{v}$-velocity field in the (x, z)-plane at $y = \frac{1}{2}\delta$ at the same time as the field shown in figure 9(*a*). Negative values are denoted by dashed contours and the contour intervals are $0.186u_\tau$.

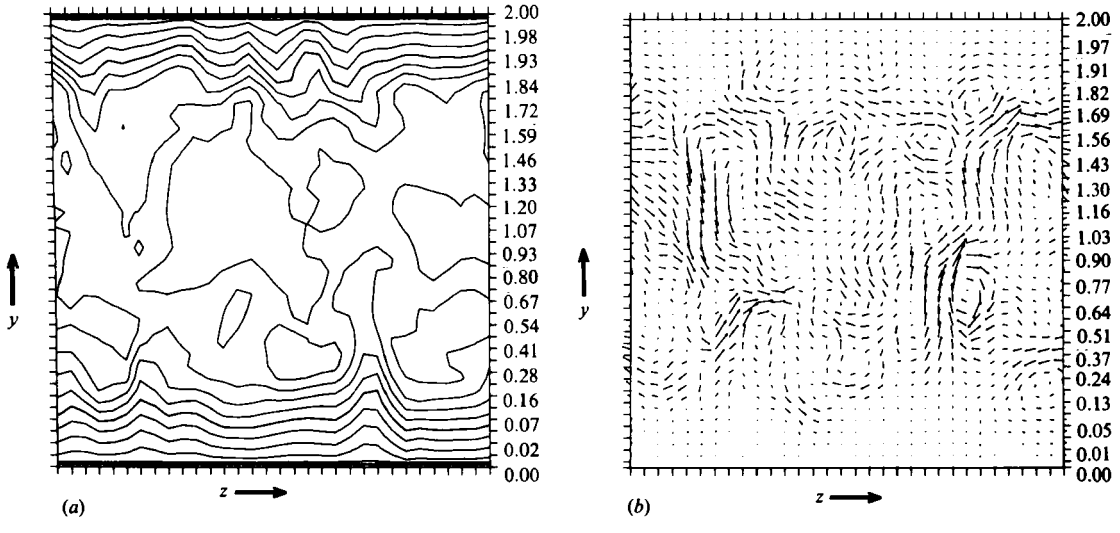

FIGURE 13. Sections of (*a*) the streamwise velocity $\bar{u}$ and (*b*) $\bar{v}$, $\bar{w}$ flow vectors in the (z, y)-plane for run A2. The time is the same as for figure 9(*a*) and the section is at the centre of the domain. Note that the y-scale allows equal distance for each mesh interval and true heights are given on the axis. The contour interval in (*a*) is $2.42u_\tau$ and the peak value of $\bar{v}$ in the vector field is $2.1u_\tau$.

of initial conditions. The flow is then found to contain significant variations on a timescale of order $10\,\delta/u_\tau$ which give fluctuations in both the resolved-scale energy and across-channel symmetry.

As noted above, in future work these conclusions regarding the role of l_0 and C_s should also be tested on the simulations of homogeneous isotropic turbulence. In its own right the present work supports the use of a Smagorinsky subgrid model with $C_s \approx 0.2$ and suggests that, if the resolved-scale turbulence should decay, increased resolution is needed to reduce l_0. The previous failures to sustain resolved-scale turbulence energy with $C_s = 0.2$, and the need to neglect deformation due to mean

shear, are attributed to the implied values of C_s being $\gtrsim 0.03\delta$ and too large to allow sustained motions. The need for adequate initial conditions when l_0 is $\approx 0.02\delta$ may also have contributed to these failures. Although we suggest that values of $C_s \approx 0.2$ and neglect of mean shear are not desirable we acknowledge that useful results have been obtained with such features. We regard this success as no more than an indication that, within certain bounds, the dominant resolved-scale motions are not too sensitive to the subgrid model.

REFERENCES

ANTONOPOULOS-DOMIS, M. 1981 Large-eddy simulation of a passive scalar in isotropic turbulence. *J. Fluid Mech.* **104**, 55–79.

BARDINA, J., FERZIGER, J. H. & REYNOLDS, W. C. 1983 Improved turbulence models based on large eddy simulation of homogeneous, incompressible, turbulent flows. *Stanford University Rep.* TF-19.

CAMBON, C., JEANDEL, D. & MATHIEU, J. 1981 Spectral modelling of homogeneous non-isotropic turbulence. *J. Fluid Mech.* **104**, 247–62.

COMTE-BELLOT, G. 1963 Contribution à l'étude de la turbulence de conduite. Doctoral thesis, University of Grenoble.

DEARDORFF, J. W. 1970*a* On the magnitude of the subgrid-scale eddy coefficient. *J. Comp. Phys.* **7**, 120–133.

DEARDORFF, J. W. 1970*b* A numerical study of three-dimensional turbulent channel flow at large Reynolds numbers. *J. Fluid Mech.* **41**, 453–480.

DEARDORFF, J. W. 1974 Three-dimensional numerical study of the height and mean structure of a heated planetary boundary layer. *Boundary-Layer Met.* **7**, 81–106.

HUSSAIN, A. K. M. F. & REYNOLDS, W. C. 1975 Measurements in fully developed turbulent channel flows. *Trans. ASME* I: *J. Fluids Engng* **97**, 568–578.

KALNAY DE RIVAS, E. 1972 On the use of non-uniform grids in finite-difference equations. *J. Comp. Phys.* **10**, 202.

KRAICHNAN, R. H. 1976 Eddy viscosity in two and three-dimensions. *J. Atmos. Sci.* **33**, 1521–1536.

KWAK, D., REYNOLDS, W. C. & FERZIGER, J. H. 1975 Three-dimensional time-dependent computation of turbulent flow. *Stanford University Rep.* TF-5.

LAUFER, J. 1951 Investigation of turbulent flow in a two-dimensional channel. *NACA rep.* 1053.

LAUNDER, B. E. & SPALDING, D. B. 1972 *Mathematical Models of Turbulence.* Academic.

LEONARD, A. 1974 Energy cascade in large-eddy simulations of turbulent fluid flows. *Adv. Geophys.* **18**A, 237–248.

LESLIE, D. C. & QUARINI, G. L. 1979 The application of turbulence theory to the formulation of subgrid modelling procedures. *J. Fluid Mech.* **91**, 65–91.

LILLY, D. K. 1967 The representation of small-scale turbulence in numerical simulation experiments. In *Proc. IBM Scientific Computing Symposium on Environmental Sciences, IBM Form No.* 320-1951, pp. 195–210.

MASON, P. J. & SYKES, R. I. 1978 A simple Cartesian model of boundary layer flow over topography. *J. Comp. Phys.* **28**, 198–210.

MCMILLAN, O. J. & FERZIGER, J. H. 1979 Direct testing of subgrid-scale models. *AIAA J.* **17**, 1340–1346.

MOIN, P. & KIM, J. (M & K) 1982 Numerical investigation of turbulent channel flow. *J. Fluid Mech.* **118**, 341–377.

MOIN, P., REYNOLDS, W. C. & FERZIGER, J. H. 1978 Large-eddy simulation of incompressible turbulent channel flow. *Rep. No.* TF-12 Dept. of Mech. Engng, Stanford University.

ORSZAG, S. A. & KELLS, L. C. 1980 Transition to turbulence in plane Poiseuille and plane Couette flow. *J. Fluid Mech.* **96**, 159–205.

PIACSEK, S. A. & WILLIAMS, G. P. 1970 Conservation properties of convection difference schemes. *J. Comp. Phys.* **6**, 392–405.

ROACHE, P. J. 1972 *Computational Fluid Dynamics.* Albuquerque: Hermosa.

RUNSTODLER, P. W., KLINE, S. J. & REYNOLDS, W. C. 1963 An investigation of the flow structure of the turbulent boundary layer. *Dept Mech. Eng. Stanford University Rep.* MD-8.

SABOT, J. & COMTE-BELLOT, G. 1976 Intermittency of coherent structures on the core region of fully developed turbulent pipe flow. *J. Fluid Mech.* **74**, 767.

SCHUMANN, U. 1975 Subgrid-scale model for finite difference simulations of turbulent flows in plane channels and annuli. *J. Comp. Phys.* **18**, 376–404.

SMAGORINSKY, J. 1963 General circulation experiments with the primitive equations: 1. The basic experiment. *Mon. Wea. Rev.* **91**, 99–164.

TOWNSEND, A. A. 1976 *The Structure of Turbulent Shear Flow.* Cambridge University Press.

VAN DRIEST, E. R. 1956 On turbulent flow near a wall. *J. Aero. Sci.* **23**, 1007–1011.

WILLIAMS, G. P. 1969 Numerical integration of the three-dimensional Navier–Stokes equations for incompressible flow. *J. Fluid Mech.* **37**, 727–750.